Electronic Supplementary Material (ESI) for Physical Chemistry Chemical Physics.

Supplementary Material - Diversity of protonated mixed pyrene-water clusters investigated by collision induced dissociation

Arya M Nair,[†,‡] Héloïse Leboucher,[¶] Lorris Toucouere,[¶] Sébastien Zamith,[*,†] Christine Joblin,[‡] Jean-Marc L'Hermite,[†] Alexandre Marciniak,[†] and Aude Simon[¶]

†*Laboratoire Collisions Agrégats Réactivité (LCAR/FERMI), UMR5589, Université Toulouse III - Paul Sabatier and CNRS, 118 Route de Narbonne, F-31062 Toulouse, France*

‡*Institut de Recherche en Astrophysique et Planétologie (IRAP), UMR5277, Université Toulouse III - Paul Sabatier and CNRS, CNES, 9 avenue du Colonel Roche, F-31028 Toulouse, France*

¶*Laboratoire de Chimie et Physique Quantiques LCPQ/FERMI, Université Toulouse III - Paul Sabatier and CNRS, 118 Route de Narbonne, F-31062 Toulouse, France*

E-mail: sebastien.zamith@irsamc.ups-tlse.fr

Abstract

1 Comparison at different collision energy and with different collision gases

CID experiments of $(Py)_m(H_2O)_nH^+$ [m =1-3, n = 1-10] on collision with different collision gases at E_{COM} = 7.5 and 15 eV was performed. Summary of the experiments performed is given in Table S1. In this supplementary section, we provide the comparison between the CID experiments carried out at different COM collision energies (15 eV) and with different collision gases.

Table S1: Summary of the CID experimental conditions. E_{COM} is the COM collision energy and E_k is the laboratory frame kinetic energy.

Species	Collision gas	$E_{COM}(eV)$	$E_k(eV)$
$(Py)_1(H_2O)_nH^+$ n=[1-10]	Neon	7.5	90-151
	Argon	7.5	49-79
$(Py)_1(H_2O)_nH^+$ n=[1-10]	Argon	15	98-158
$(Py)_2(H_2O)_nH^+$ n=[1-6]	Argon	7.5	87-103
	Krypton	7.5	45-53
	Xenon	7.5	32-37
$(Py)_3(H_2O)_nH^+$ n=[2-6]	Xenon	7.5	44-48

1.1 Comparison with different collision gases

1.1.1 $(Py)_m(H_2O)_nH^+$, m=1

Collision Induced dissociation (CID) experiments on $(Py)_1(H_2O)_nH^+$ [n=1-10] with argon at 7.5 eV centre of mass collision energy was discussed in the main article. The experiment was also carried out with neon at the same COM collision energy. Figure S1 presents the comparison of the branching ratios plotted as a function of number of water molecules attached on $(Py)_1(H_2O)_nH^+$ [n=1-10] with neon and argon.

In the figure S1, the two channels represents the the branching ratios for the loss of water molecules (BR_1) and water with pyrene molecules (BR_0) (same as the detection of protonated water clusters) respectively. Upon collision with neon, up to n=2, the probability

to remove neutral pyrene from the cluster is negligible. This indicates that the waters are removed from the cluster and the proton prefers to stay with the fragments containing pyrene. But starting from n=3, the probability to loose both water and pyrene are around 60% and 40% and from n=4 onwards these probabilities are almost similar (around 50%). This means that from n=3 onwards,it is equally probable to have proton on both types of fragments. From the figure S1, it can be observed that the branching ratios on collision with neon are similar to that with argon. The small discrepencies between them could results from the deflections as described in the main text. Hence changing collision gases has much less influence on the fragmentation pattern.

1.1.2 $(Py)_m(H_2O)_nH^+$, m=2

The experiments on $(Py)_2(H_2O)_nH^+$ [n=1-6] with argon at 7.5 eV was discussed earlier. Here we provide the results on collision with krypton and xenon at same collision energy.

In order to understand the impact of different gases on the fragmentation of clusters, the fragmentation pattern resulting from CID with argon, krypton and xenon are presented in figure S2. The bunch of black, red and blue peaks corresponds to the detection of fragments $(H_2O)_xH^+$, $(Py)_1(H_2O)_xH^+$ and $(Py)_2(H_2O)_xH^+$, respectively. Up to n=2, the protonated water clusters are not present and they starts to appear from n=3 onwards for all the collision gases. For $(Py)_1(H_2O)_xH^+$ channel, $(Py)_1(H_2O)_3H^+$ is more intense than the neighbouring fragments. Also for $(Py)_2(H_2O)_xH^+$ fragments, $(Py)_2(H_2O)_1H^+$ is the least stable fragment in all the three cases. Although the key features remain similar for all collision gases, some difference arises for the loss of all water fragments channels, namely the detection of PyH^+ and $(Py)_2H^+$ fragments. As we go from lighter to heavier colliders, the intensity of these peaks are reduced which can be explained in the light of deflections (see main text for more details).

Figure S3 represents the branching ratios plotted as a function of the number of water molecules attached. BR_0, BR_1 and BR_2 are the branching ratios for detection of $(H_2O)_xH^+$,

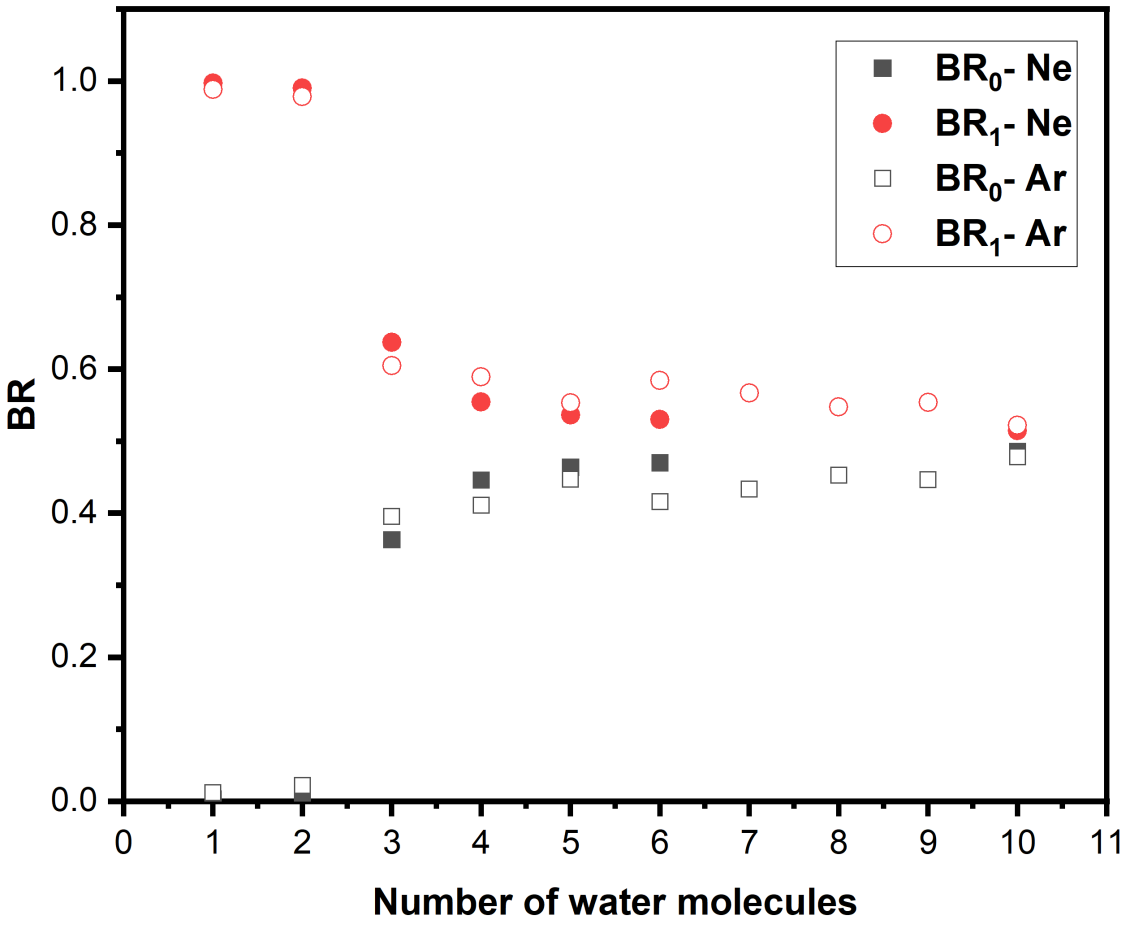

Figure S1: Comparison of the branching ratios plotted as a function of number of water molecules attached on $(Py)_1(H_2O)_nH^+$ [n=1-10] with neon and argon

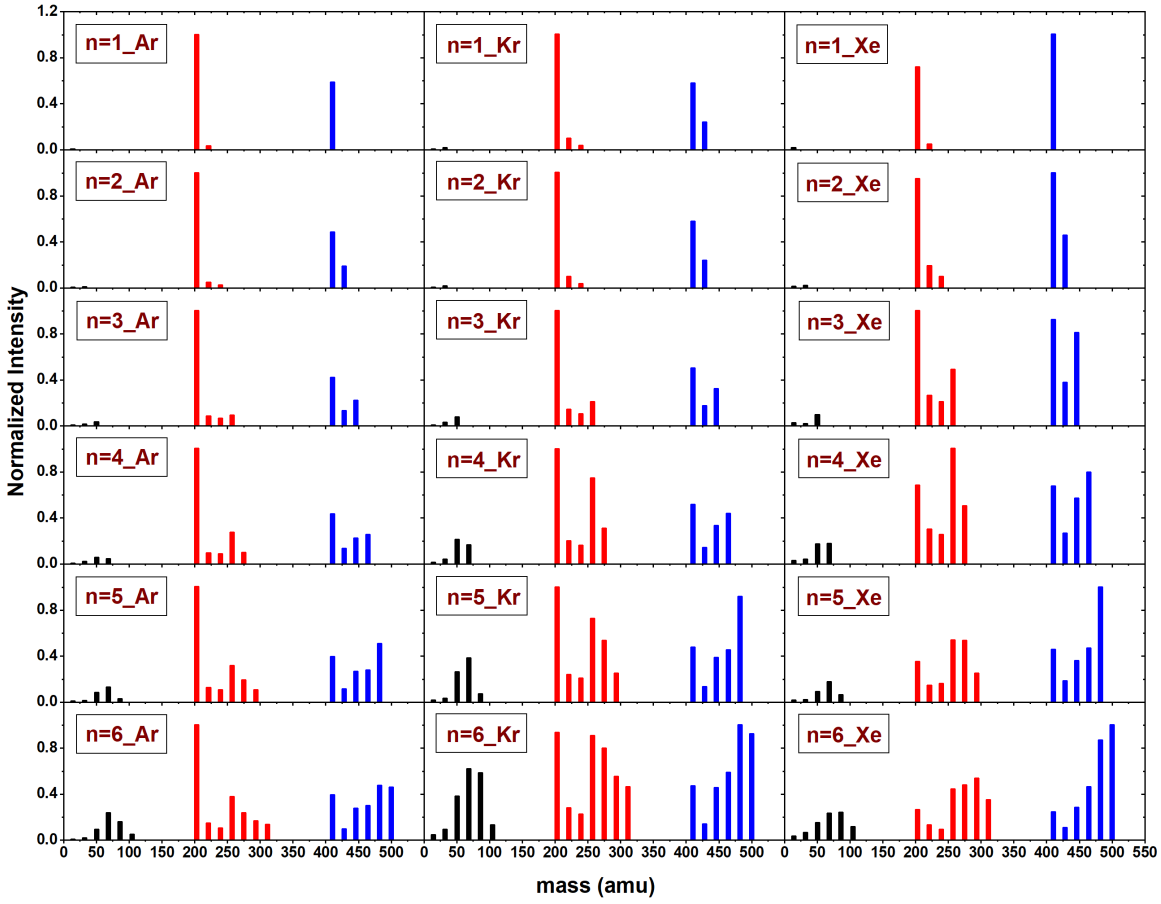

Figure S2: Fragment distribution comparison on $(Py)_2(H_2O)_nH^+$ [n=1-6] with different collision gases namely Argon, Krypton and Xenon.

$(Py)_1(H_2O)_xH^+$ and $(Py)_2(H_2O)_xH^+$ fragments, respectively.

From the figure it can be observed that for BR_0 and BR_1, the curves for the argon and krypton are rather similar whereas the xenon case appears to be different. The difference could arise from the fact that the xenon having a much heavier mass compared to the others, deflections are expected to be more likely. Apart from this, it is clear that BR_2 is slowly evolving for all the collision gases starting from n = 3 onwards. The BR_1 starts to decrease from n = 5 and for the BR_0, the branching ratios decreases from n = 1 to 4 and then increases.

Here again, we find that the branching ratios remain relatively similar, whatever the collision gas is employed. Therefore, our results appear to be quite robust against the collisional energy transfer details.

1.2 Comparison at different collision energy

CID experiments were repeated on $(Py)_1(H_2O)_nH^+$ [n = 1-10] with Argon at 15 eV center of mass collision energy. The experiment at 7.5 eV is extensively described in the main paper. Figure S4 represents the branching ratios plotted as a function of the number of water molecules attached for two COM collision energies namely 15 eV and 7.5 eV. The branching ratios BR_1 and BR_0 corresponds to the loss of water molecules only and the loss of both pyrene and water molecules (detection of protonated water clusters), respectively.

From the figure S4, it can be observed that the overall behaviour looks similar for both collision energies. For n=1-2, BR_0 is zero indicating that we do not detect any protonated water clusters. But starting from n=3, the branching ratios are getting almost equal, although there is a minor difference in the behaviour starting from n=3 onwards. For 7.5 eV, BR_0 and BR_1 are constantly approching each other from n=3-10. But for 15 eV the branching ratios are getting closer till n=5 and are then crossing each other. This difference in behaviour with different collision energies can occur due to different reasons. One, since we put different collision energies (7.5 eV and 15 eV) on the same system, the energy given to

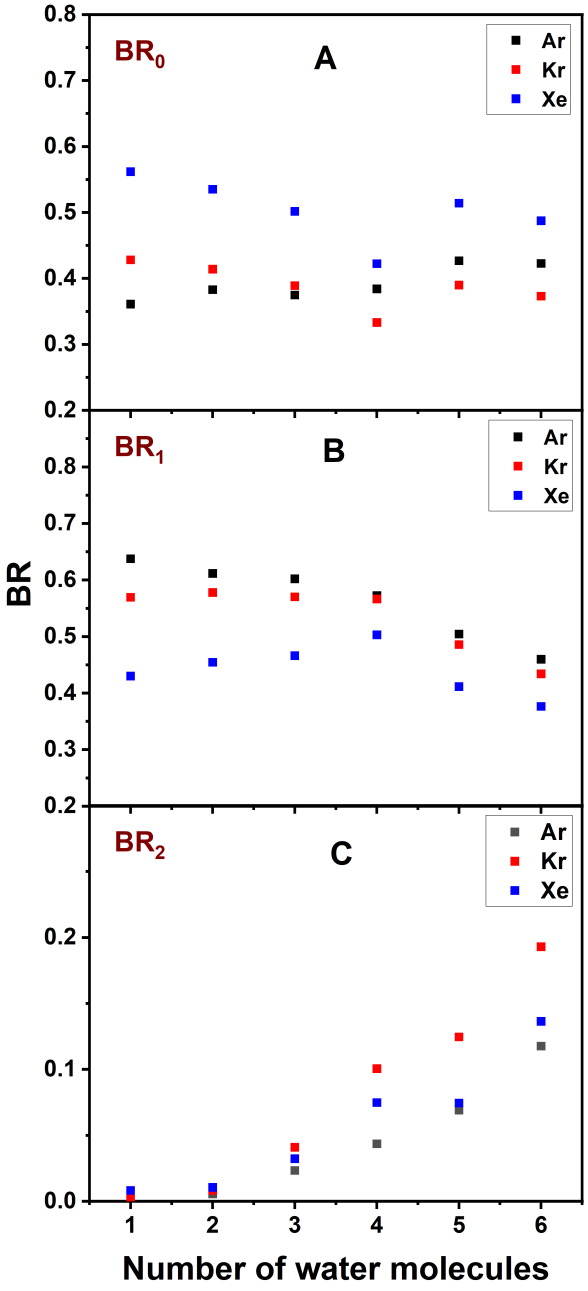

Figure S3: Comparison of the branching ratios plotted as a function of number of water molecules attached on $(Py)_2(H_2O)_nH^+$ with different collision gases(Argon, Krypton and Xenon)

the cluster will be quite different and at such high energy as 15 eV, the system can undergo violent fragmentation resulting in the difference in fragmentation pattern. Secondly, for acquiring 15 eV COM collision energy we have to go higher in the lab frame kinetic energy which reduces the quality of mass selection. So this could explain the slight change in the behaviour upon changing the collision energies.

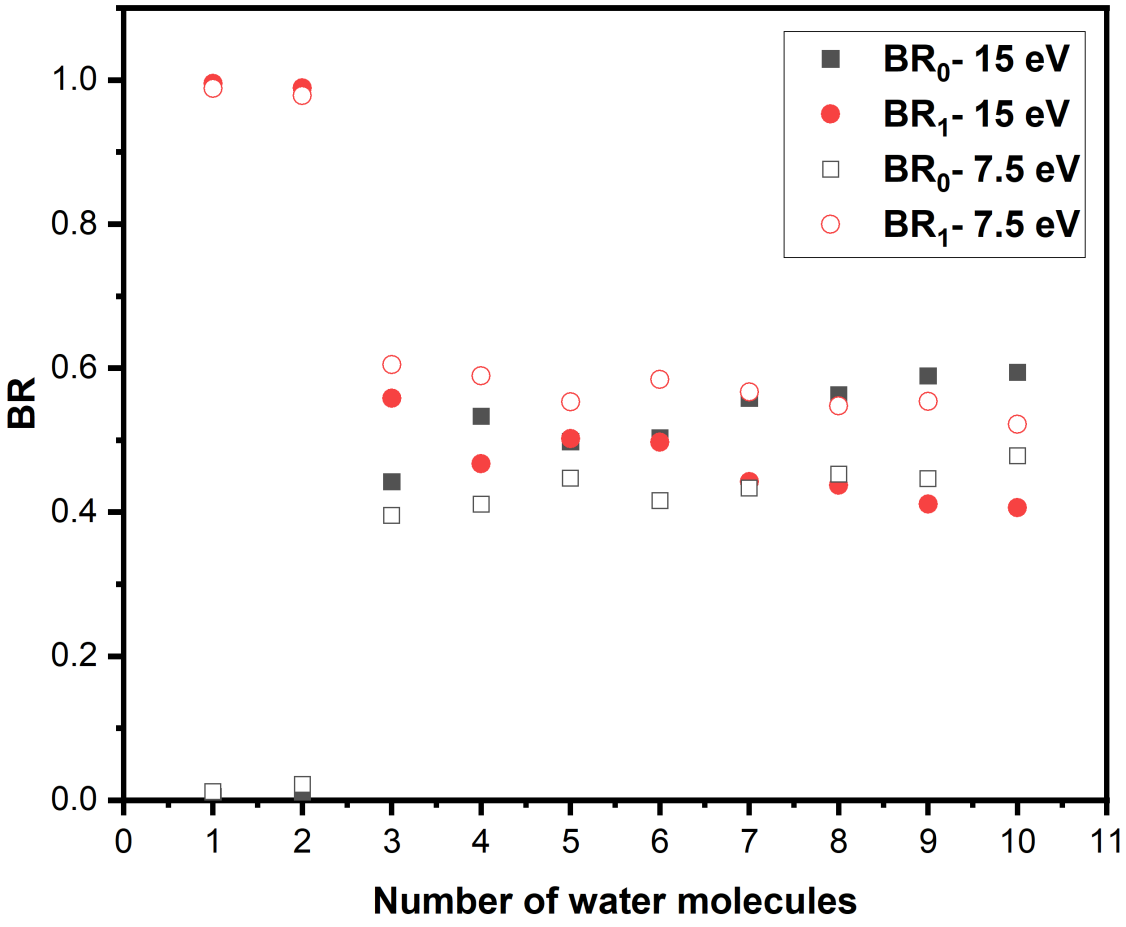

Figure S4: Comparison of the branching ratios plotted as a function of number of water molecules attached on $(Py)_1(H_2O)_nH^+$ [n=1-10] with argon at 15 eV and 7.5 eV.

2 Total fragmentation cross section

Total fragmentation cross sections of $(Py)_m(H_2O)_nH^+$ [m=1-3,n=1-10] as a function of number of water molecules attached are plotted in figureS5. We observe that the cross-sections are increasing as we go from 1 pyrene to 3 pyrene units. For $(Py)_1(H_2O)_nH^+$, the fragmentation cross-section is increasing from 30 Å^2 to 85 Å^2 with the number of water molecules attached. For $(Py)_2(H_2O)_nH^+$, the cross-section have almost a constant value around 70 Å^2. Cross-sections for $(Py)_3(H_2O)_nH^+$ is also slowly evolving with the number of water molecules attached.

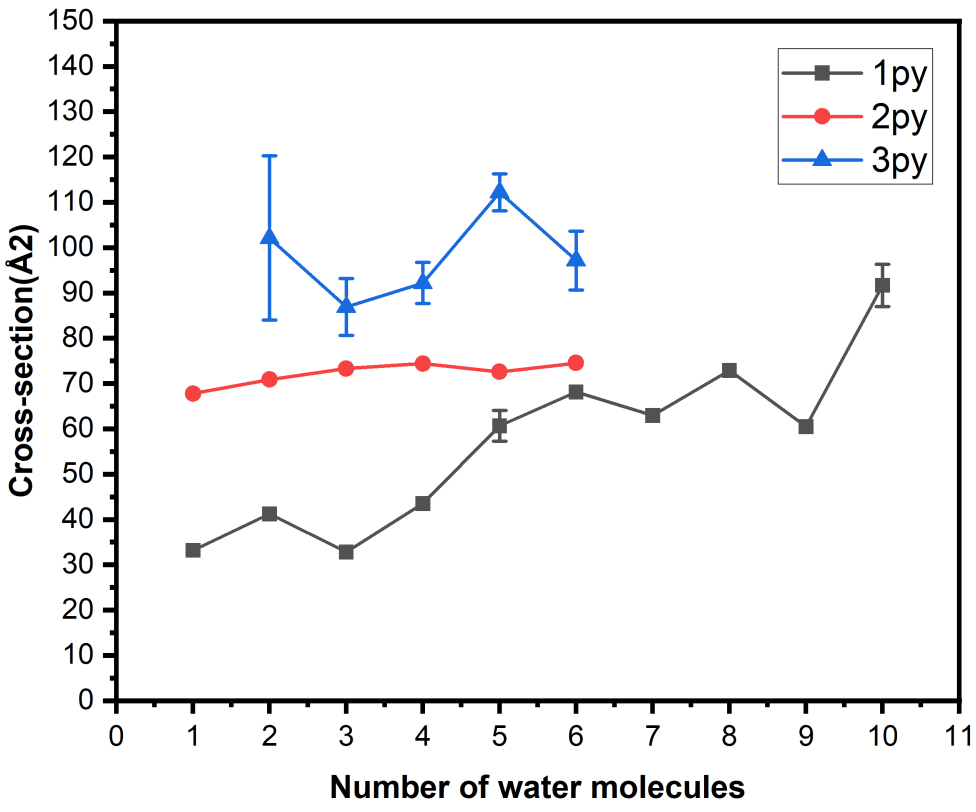

Figure S5: Cross section plotted as a function of number of water molecules attached on $(Py)_m(H_2O)_nH^+$ [m=1-3,n=1-10]. Error bars correspond to one standard deviation.

3 Comparison of contribution from m=1 in m=2.

As described in the main text, we suspect there was some contribution of m=1 in m=2 fragmentation as the $(H_2O)_xH^+$ $[BR_0]$ and $(Py)_1(H_2O)_xH^+$ $[BR_1]$ peaks looks similar for both the cases. To separate this contribution, we have normalized BR_0 and BR_1 peaks of m=2 with BR_0 of m=1. An example of this normalization and the results for $(Py)_2(H_2O)_6H^+$ is given in the figure S6. The unfilled bunches of black, red and blue peaks corresponds to the $(H_2O)_xH^+$, $(Py)_1(H_2O)_xH^+$ and $(Py)_2(H_2O)_xH^+$ for m=2 respectively. The filled bunches of black and red peaks is the result of normalization by the maximum of $(H_2O)_xH^+$ in m=1 fragmentation spectra.

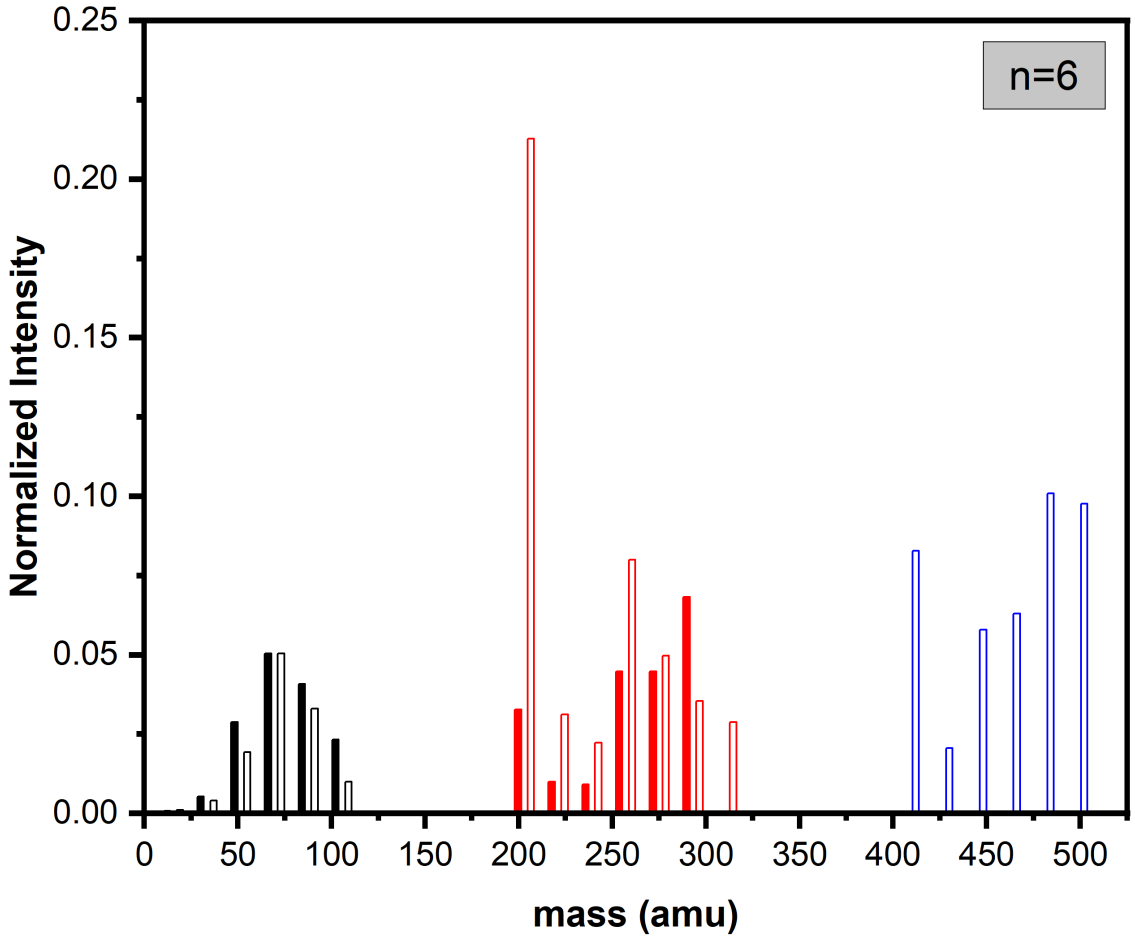

Figure S6: Mass distribution of the fragments in m=2 by normalizing BR_0 and BR_1 to $(H_2O)_nH^+$ of m=1.

4 Correction for isotope contamination

The mass selection of the parent ion do not allow us to distinguish between $(Py)_m(H_2O)_nH^+$ species and $[(Py)_m(H_2O)_n]^+$ with one pyrene molecule having a ^{13}C (^{13}Py). As mentioned in the main paper, depending on the way the clusters are produced, this contamination can be relatively high. However, using reasonable assumptions, the branching ratios BR_k can be corrected. First we assume that the fragmentation cross-section of $(Py)_m(H_2O)_nH^+$ and $[(^{13}Py)(Py)_{m-1}(H_2O)_n]^+$ are similar. Then we estimate the amount α of isotope contamination in the parent peak based on the isotopic abundance of ^{13}C and on the relative peak intensities in the TOF-MS of the produced species.

For the channel corresponding to the loss of neutral water molecules only, the correction to the sum of fragment peak intensities is simply calculated as $(1-\alpha)\sum I_{i,m}$. For the other channels, only fragments of the form $[(^{13}Py)(Py)_{k-1}(H_2O)_x]^+$ have the mass corresponding to $(Py)_k(H_2O)_xH^+$. Considering that the loss of a Py or ^{13}Py is equally probable, we derive the following expression for the isotope abundance corrected branching ratio:

$$BR_k^c = \frac{(1-\alpha)}{(1-\alpha+k\alpha/m)} \frac{\sum_i I_{i,k}}{\sum_j \frac{(1-\alpha j/m)}{(1-\alpha+j\alpha/m)} \sum_i I_{i,j}} \tag{1}$$

with $k \in [0, m]$.

For the clusters produced by introducing water upstream only, we have α= 0.08 , 0.18 and 0.32 for m=1, 2 and 3 respectively. For clusters produced by introducing water downstream we have α=0.20 and 0.44 for m=1 and 2, respectively.

The results of this correction procedure is shown in Figures S7 to S9. In Figures S7 and S8 are also plotted the corrected branching ratios when clusters are produced by adding water downstream the source.

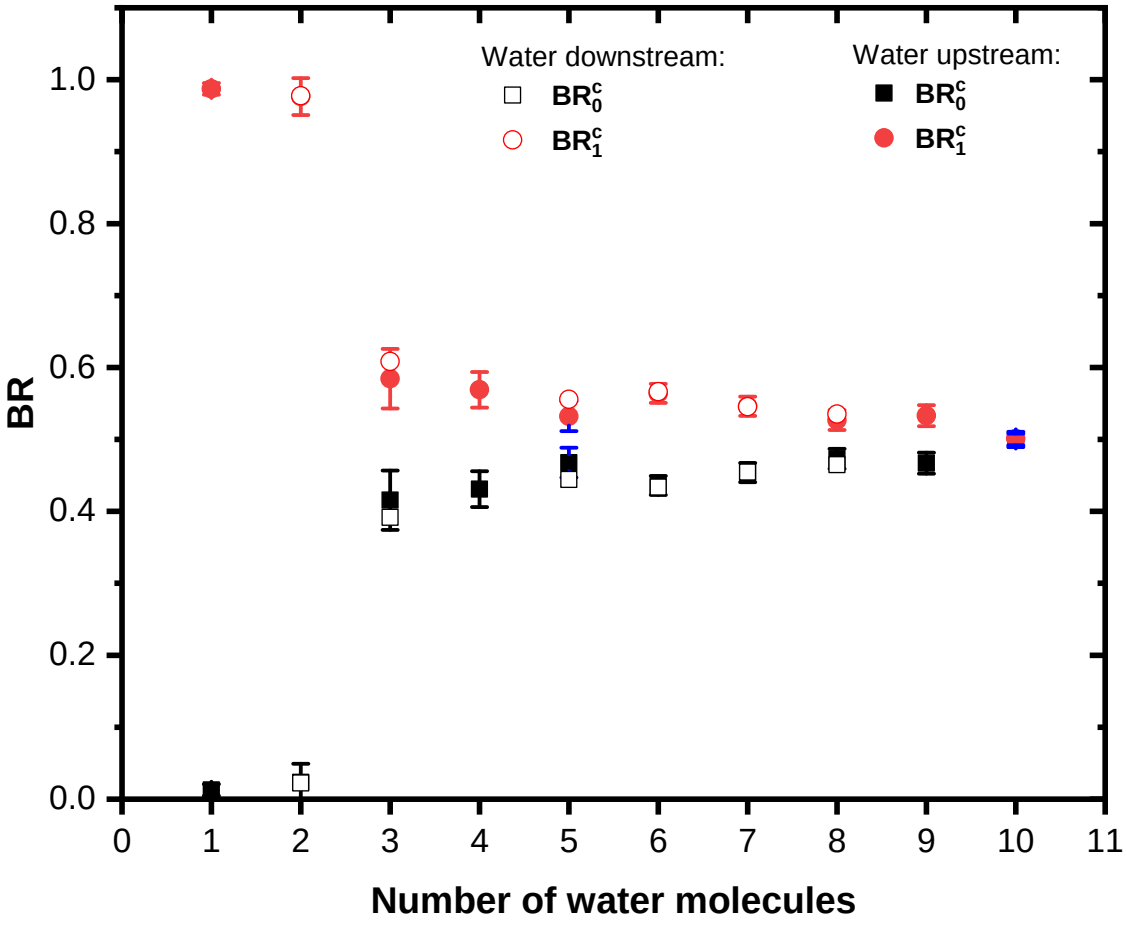

Figure S7: Isotope contamination corrected branching ratios of the fragmentation channels of $(Py)_1(H_2O)_nH^+$ as a function of the number of attached water molecules. The BR_1 channel (red circles) corresponds to the sum of $(Py)_1(H_2O)_xH^+$ fragments, with x=[0:n-1]. The BR_0 channel (black squares) gathers the protonated water clusters $(H_2O)_xH^+$, with x=[1:n]). Filled symbols are for clusters produced by adding water upstream the source. Open symbols are for clusters produced by adding water downstream the source.

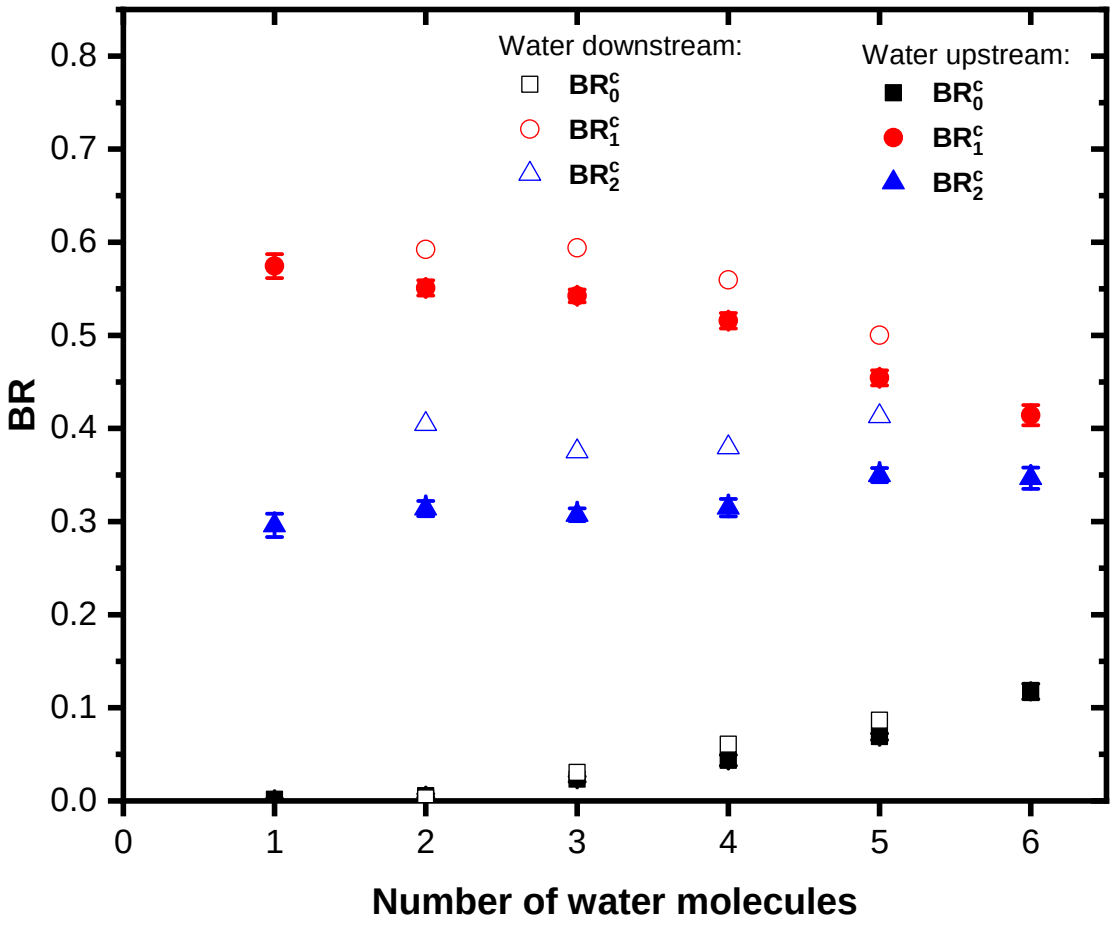

Figure S8: Isotope contamination corrected branching ratios of the fragmentation channels of $(Py)_2(H_2O)_nH^+$ as a function of the number of attached water molecules. The BR_2 channel (blue triangles) corresponds to the sum of $(Py)_2(H_2O)_xH^+$ fragments, with x=[0:n-1]. The BR_1 channel (red circles) corresponds to the sum of $(Py)_1(H_2O)_xH^+$ fragments, with x=[0:n]. BR_0 channel (black squares) gathers the protonated water clusters $(H_2O)_xH^+$, with x=[1:n]). Filled symbols are for clusters produced by adding water upstream the source. Open symbols are for clusters produced by adding water downstream the source.

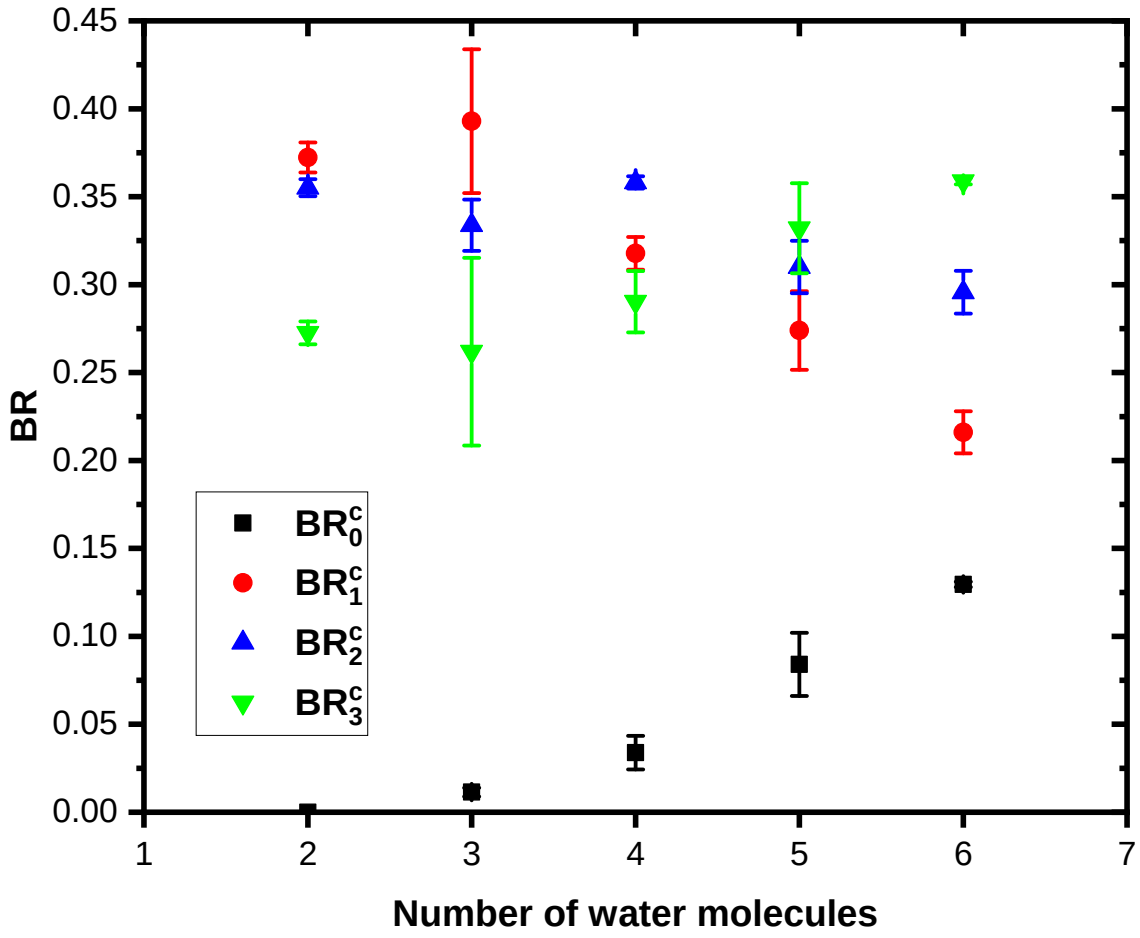

Figure S9: Isotope contamination corrected branching ratios plotted as a function of number of water molecules attached on $(Py)_3(H_2O)_nH^+$. The BR_3 channel (cyan inverted triangles) corresponds to the sum of $(Py)_3(H_2O)_xH^+$ fragments, with x=[0:n-1].The BR_2 channel (blue triangles) corresponds to the sum of $(Py)_2(H_2O)_xH^+$ fragments, with x=[0:n]. The BR_1 channel (red circles) corresponds to the sum of $(Py)_1(H_2O)_xH^+$ fragments, with x=[0:n]. BR_0 channel (black squares) gathers the protonated water clusters $(H_2O)_xH^+$, with x=[1:n]). Error bars correspond to one standard deviation, Δ_2 (as described in text).

5 Proton affinities

The PAs of Py and water clusters from previous calculations and experiments are compiled and presented in Figure S10[1–7] together the ones calculated at the DFT level in the present work. The PA of Py is about 9 eV whereas that of the water is about 7.4 eV. The PAs of water clusters increases with size and gets comparable to the one of Py for n=[2-4]. It becomes clearly greater than the Py for n≈ 3-4.[1–7]

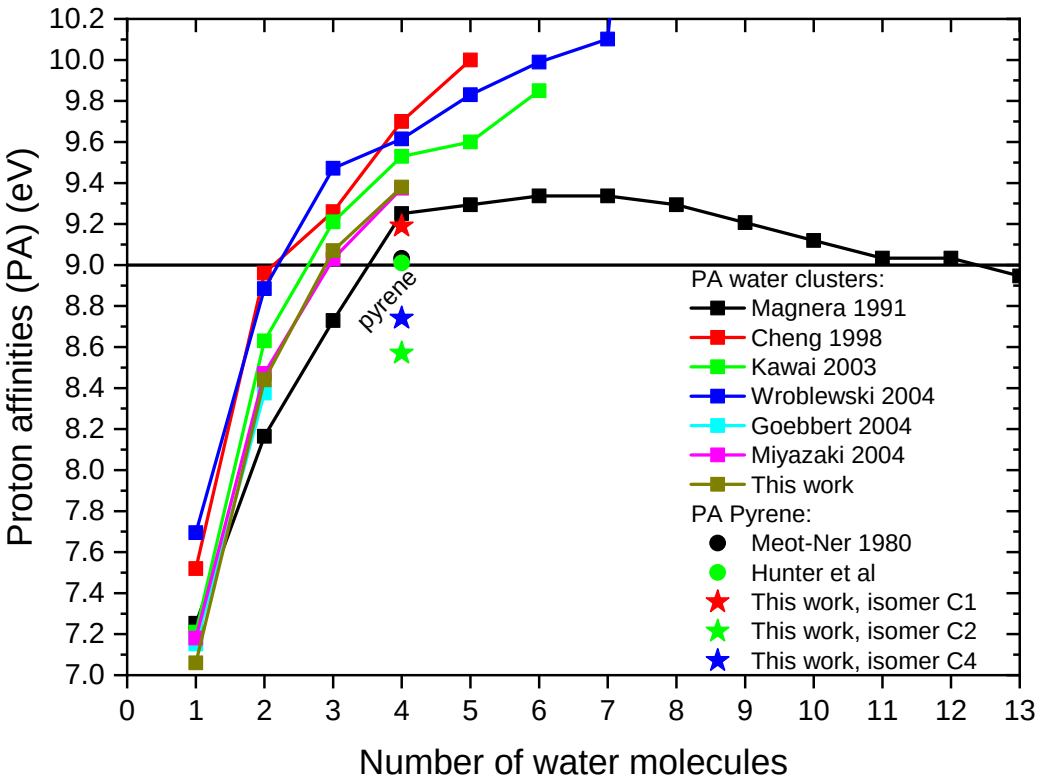

Figure S10: Comparison of proton affinities of Py and water clusters from previous theoretical and experimental works. Results of the present work at the DFT level are also included. See references in the text.

6 Calculated structures

Figure S11 is a representation of the pyrene molecules with the C1, C2 and C4 carbons atoms used as protonation sites.

Figures S12 to S23 present the lowest energy structures calculated for $(Py)_m(H_2O)_nH^+$, for m=1 and n=1-4.

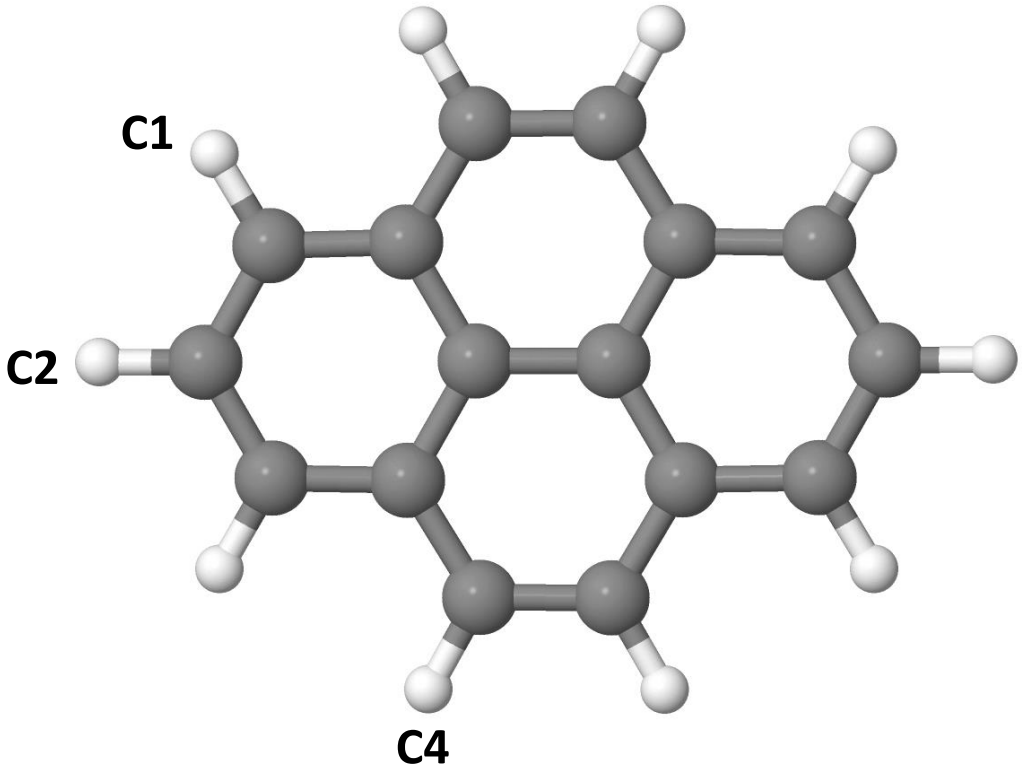

Figure S11: Numbering of the carbon atoms used for the protonation sites on the pyrene molecule.

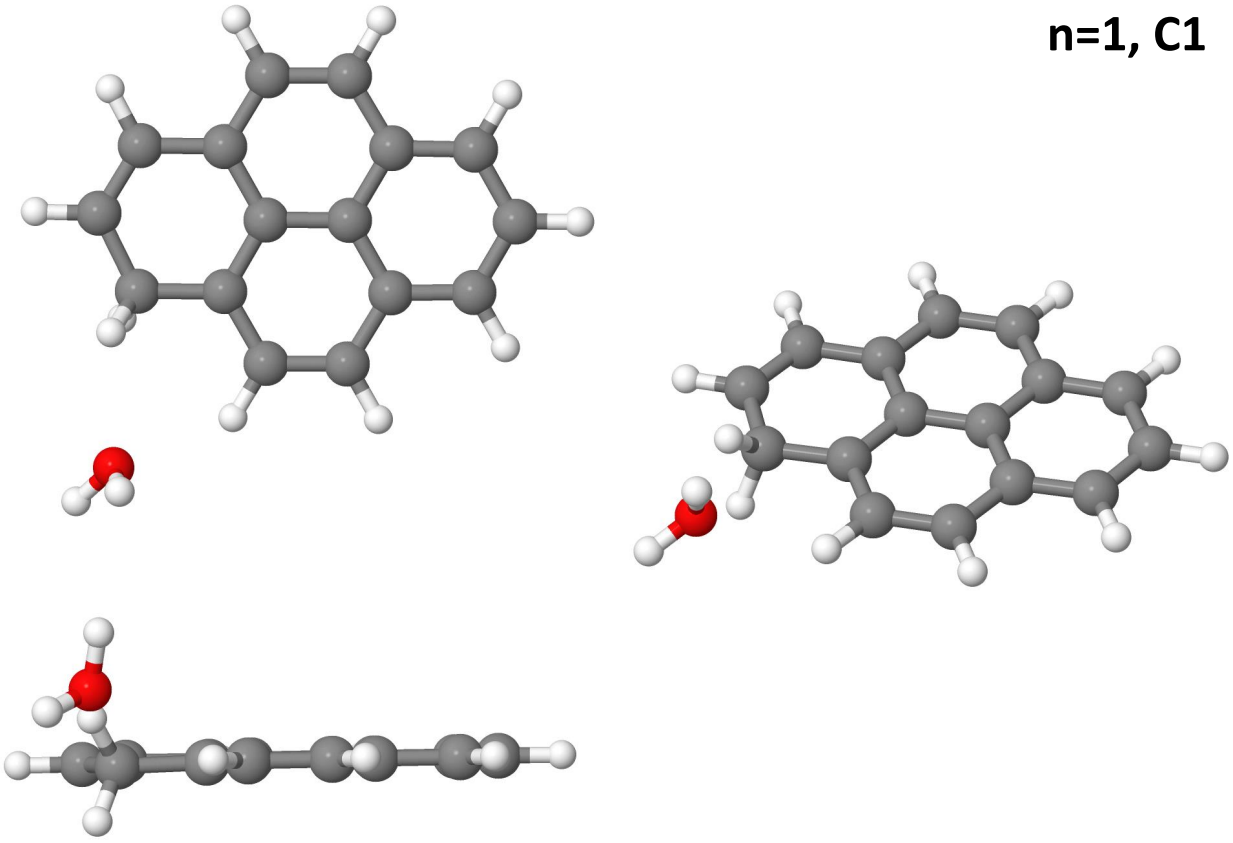

Figure S12: Different views corresponding to the lowest energy isomer obtained with a protonation site initially on C1 for n=1.

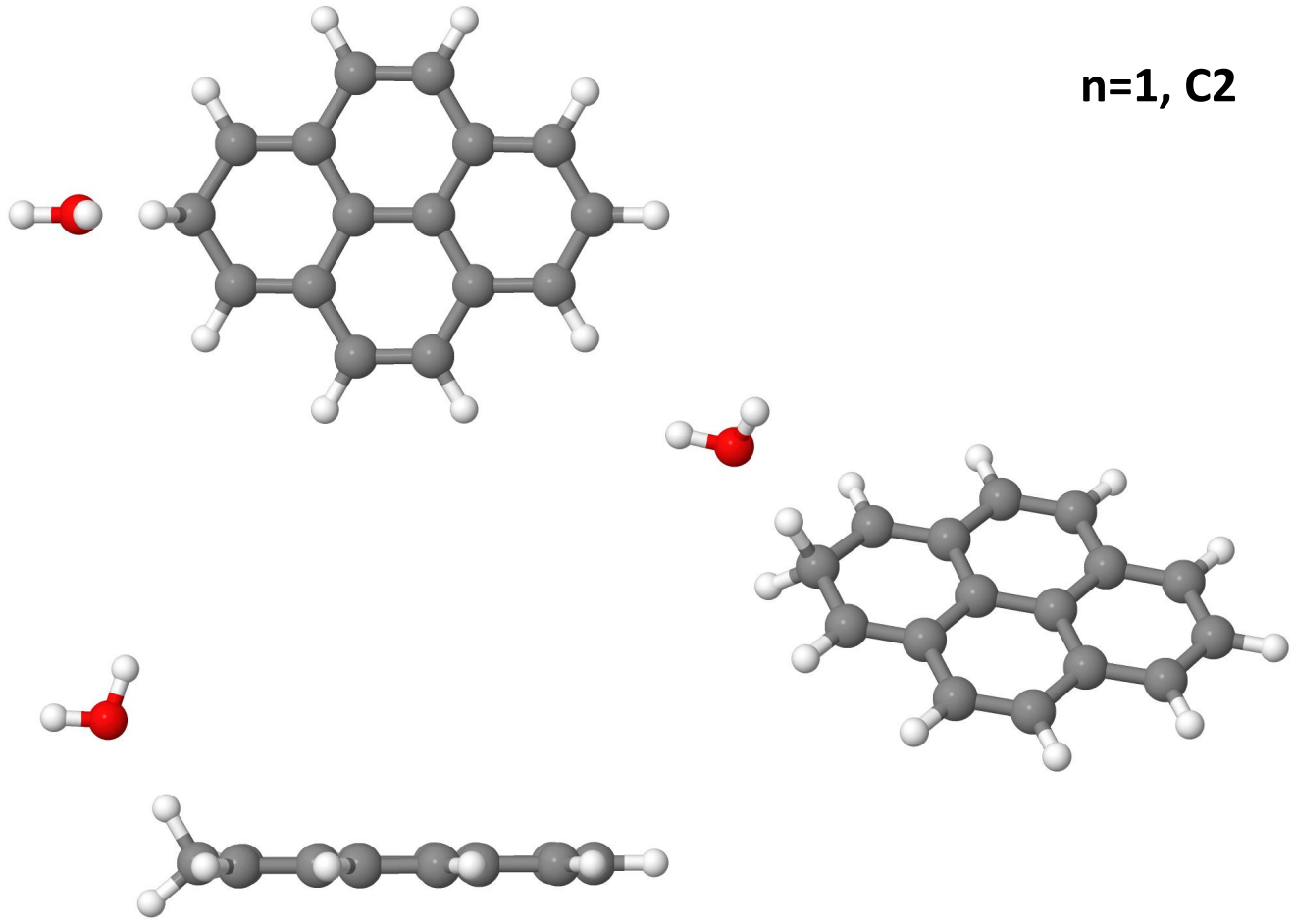

Figure S13: Different views corresponding to the lowest energy isomer obtained with a protonation site initially on C2 for n=1.

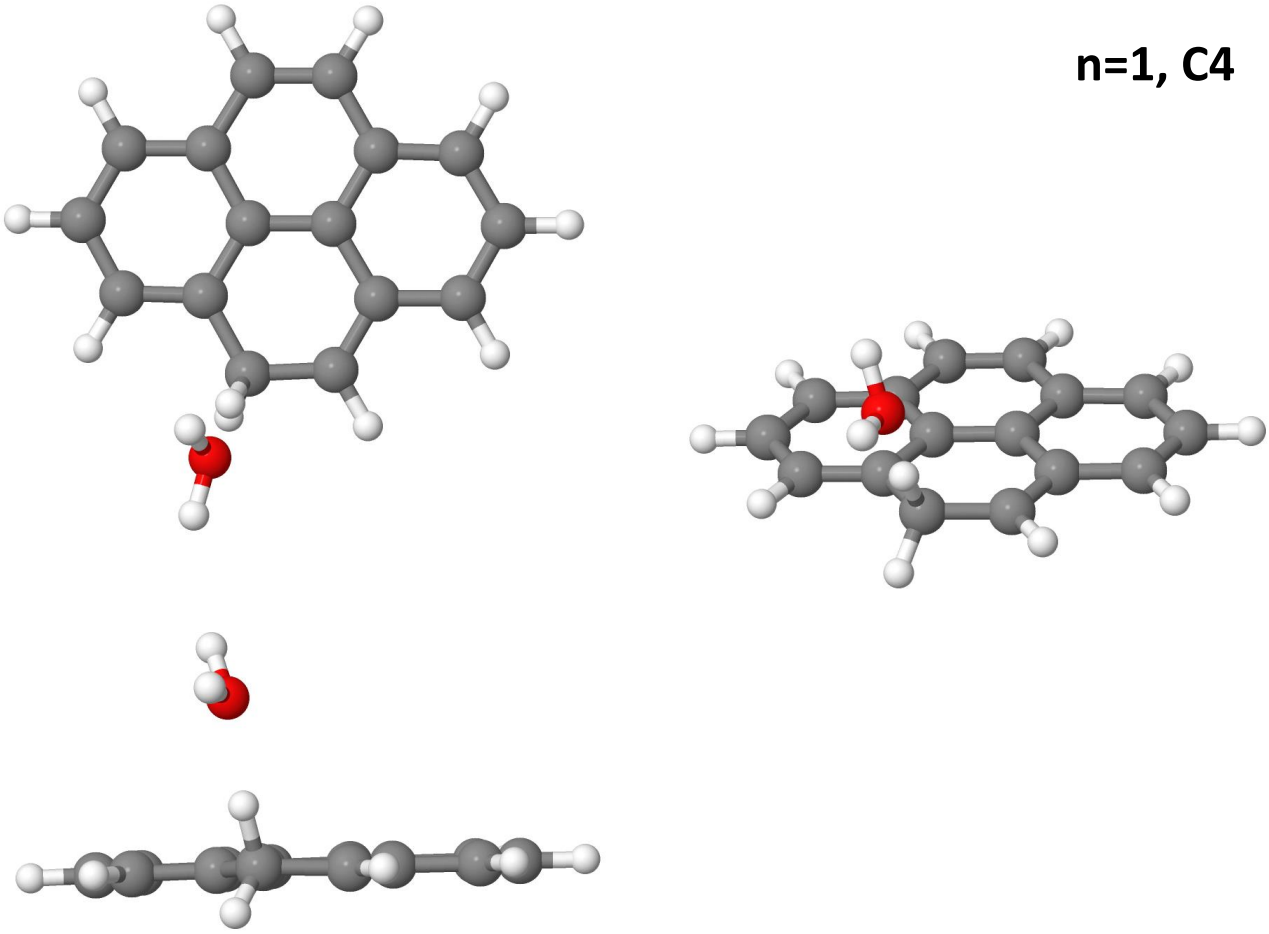

Figure S14: Different views corresponding to the lowest energy isomer obtained with a protonation site initially on C4 for n=1.

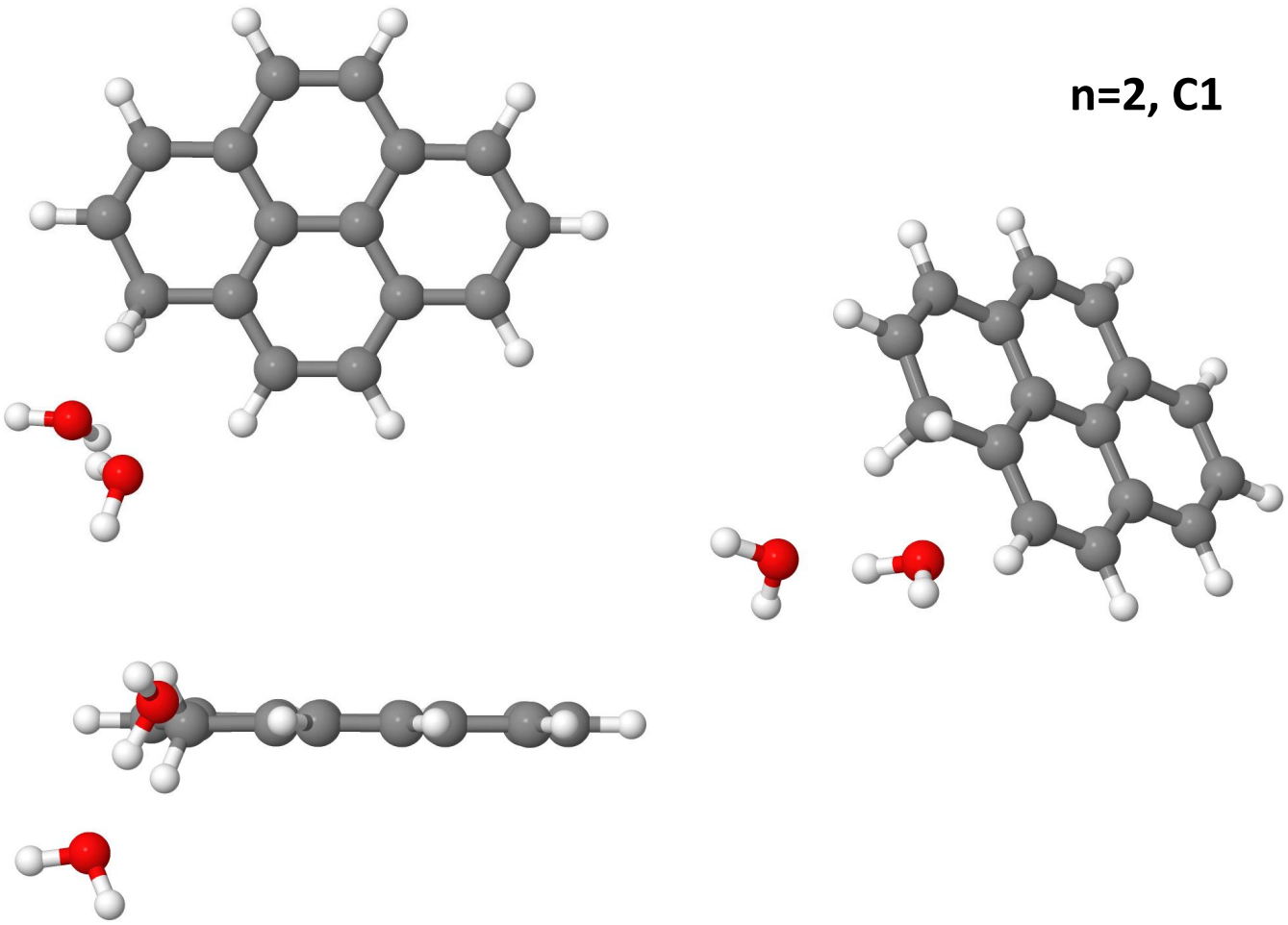

Figure S15: Different views corresponding to the lowest energy isomer obtained with a protonation site initially on C1 for n=2.

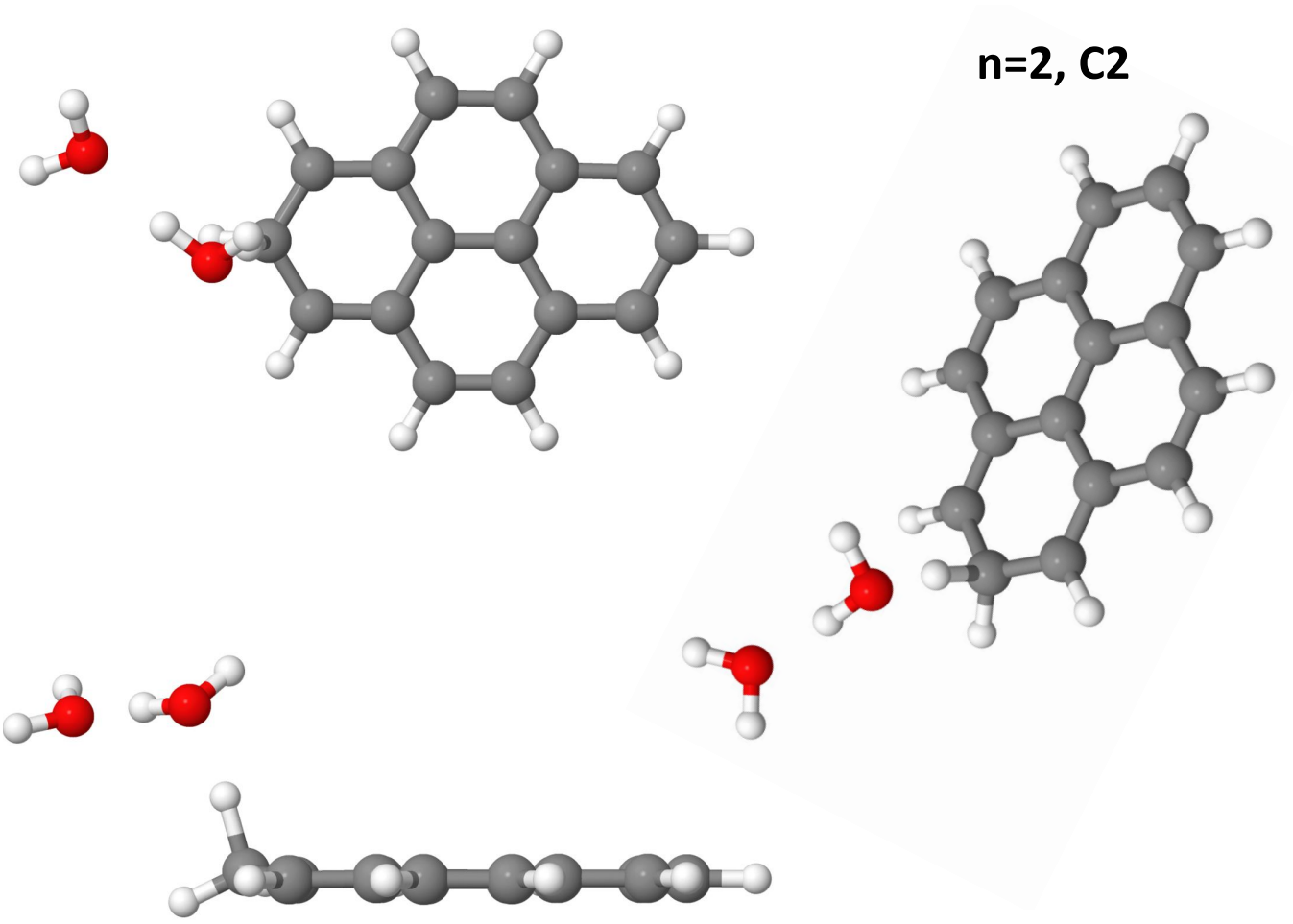

Figure S16: Different views corresponding to the lowest energy isomer obtained with a protonation site initially on C2 for n=2.

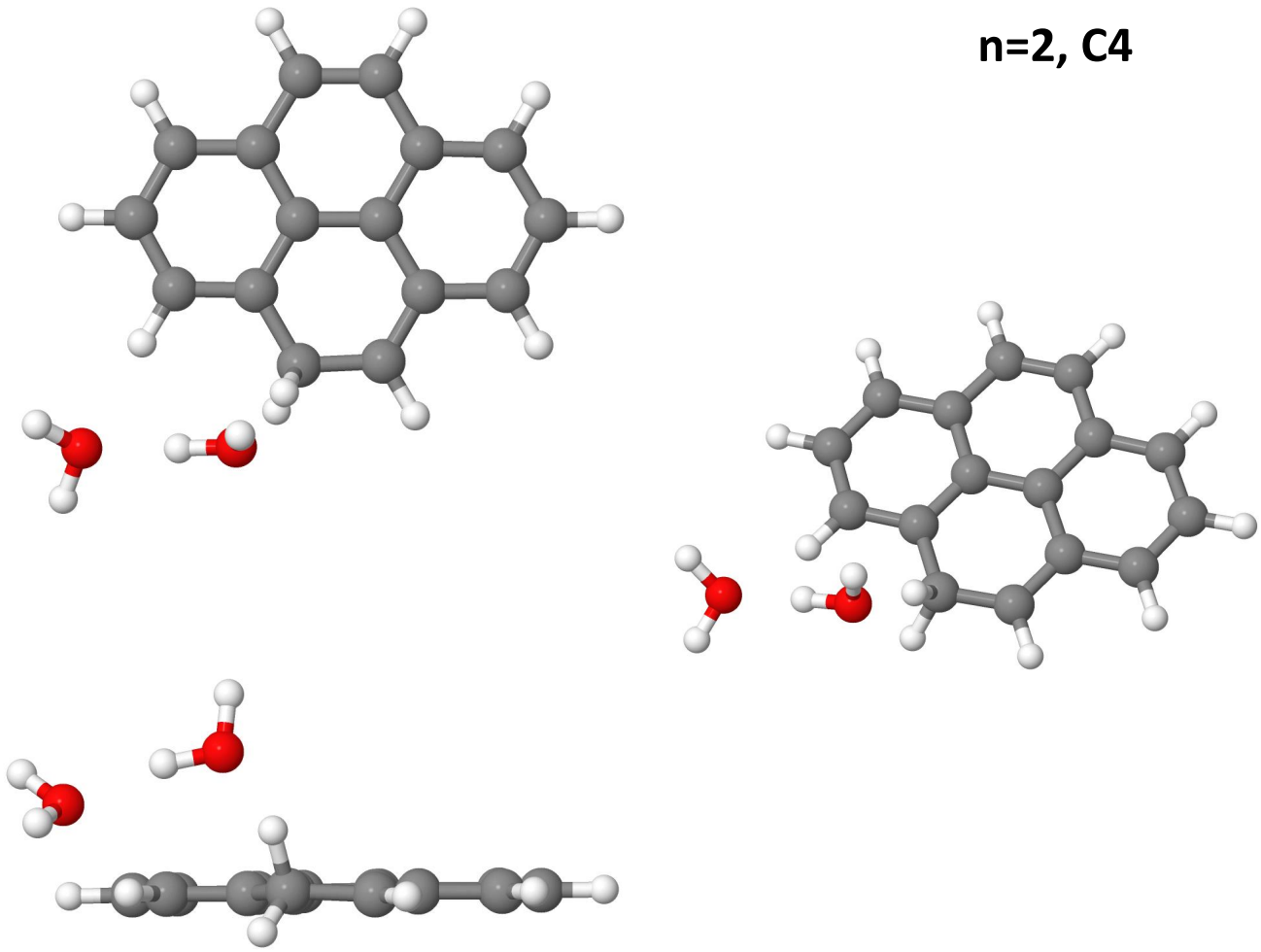

Figure S17: Different views corresponding to the lowest energy isomer obtained with a protonation site initially on C4 for n=2.

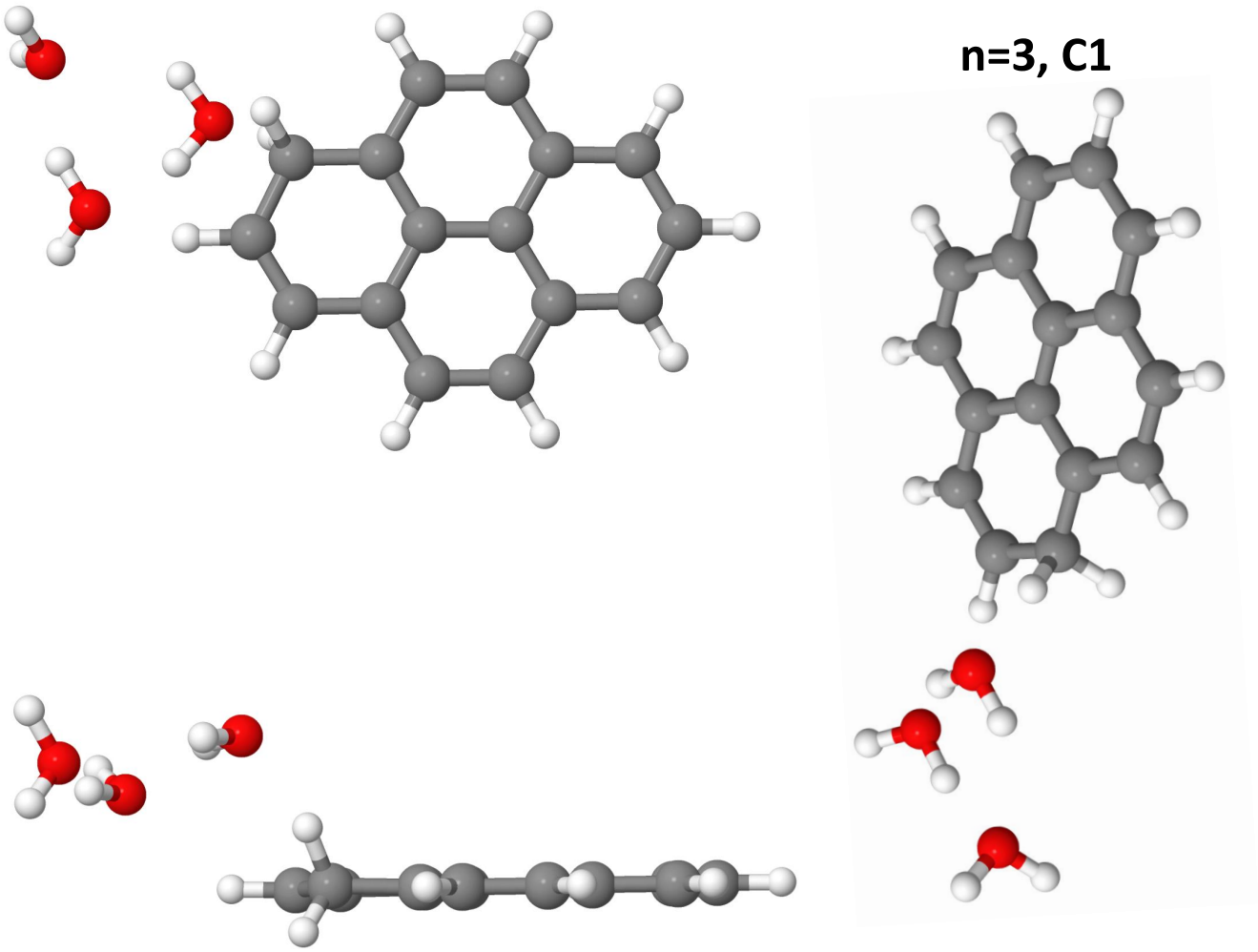

Figure S18: Different views corresponding to the lowest energy isomer obtained with a protonation site initially on C1 for n=3.

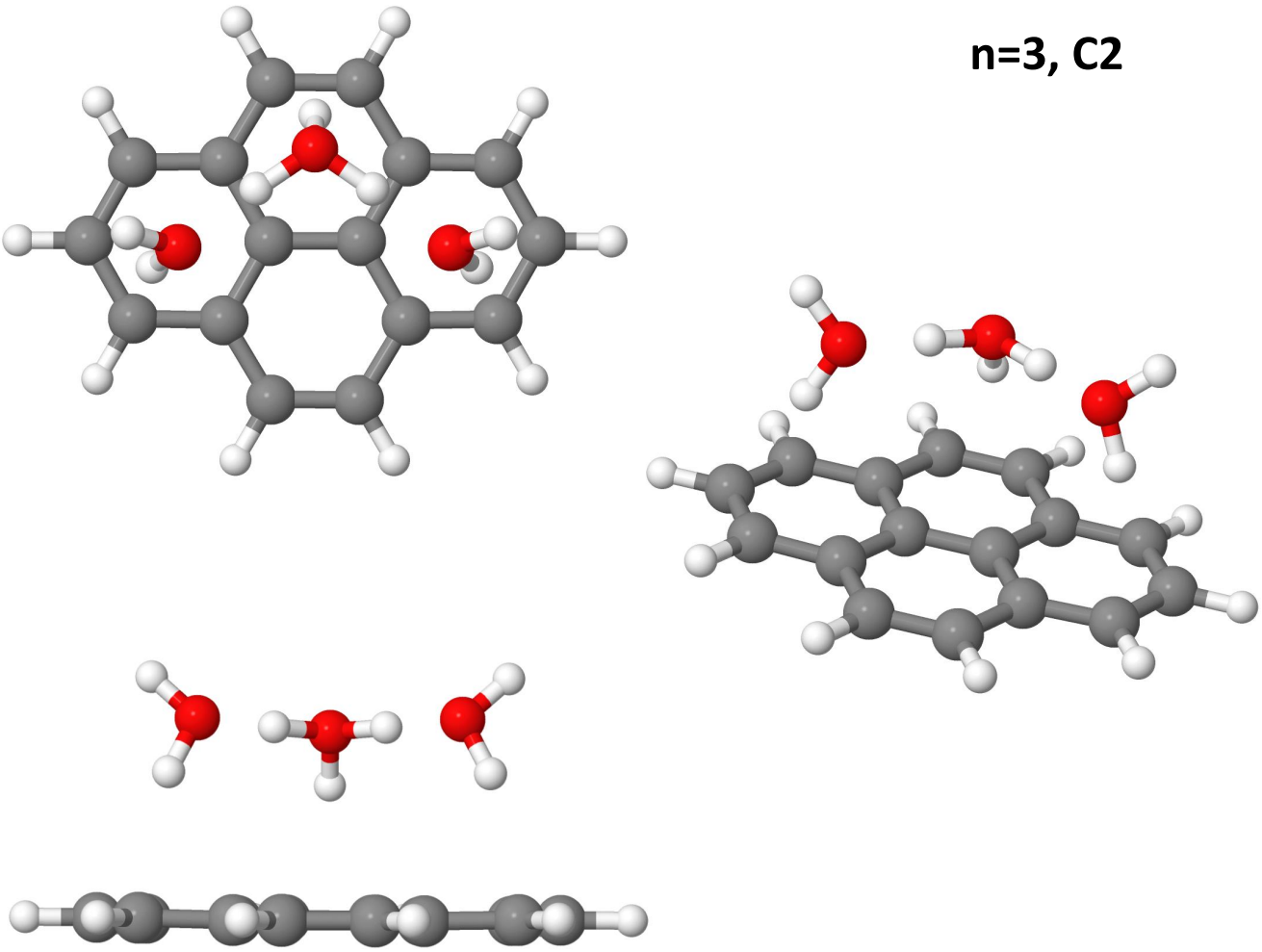

Figure S19: Different views corresponding to the lowest energy isomer obtained with a protonation site initially on C2 for n=3.

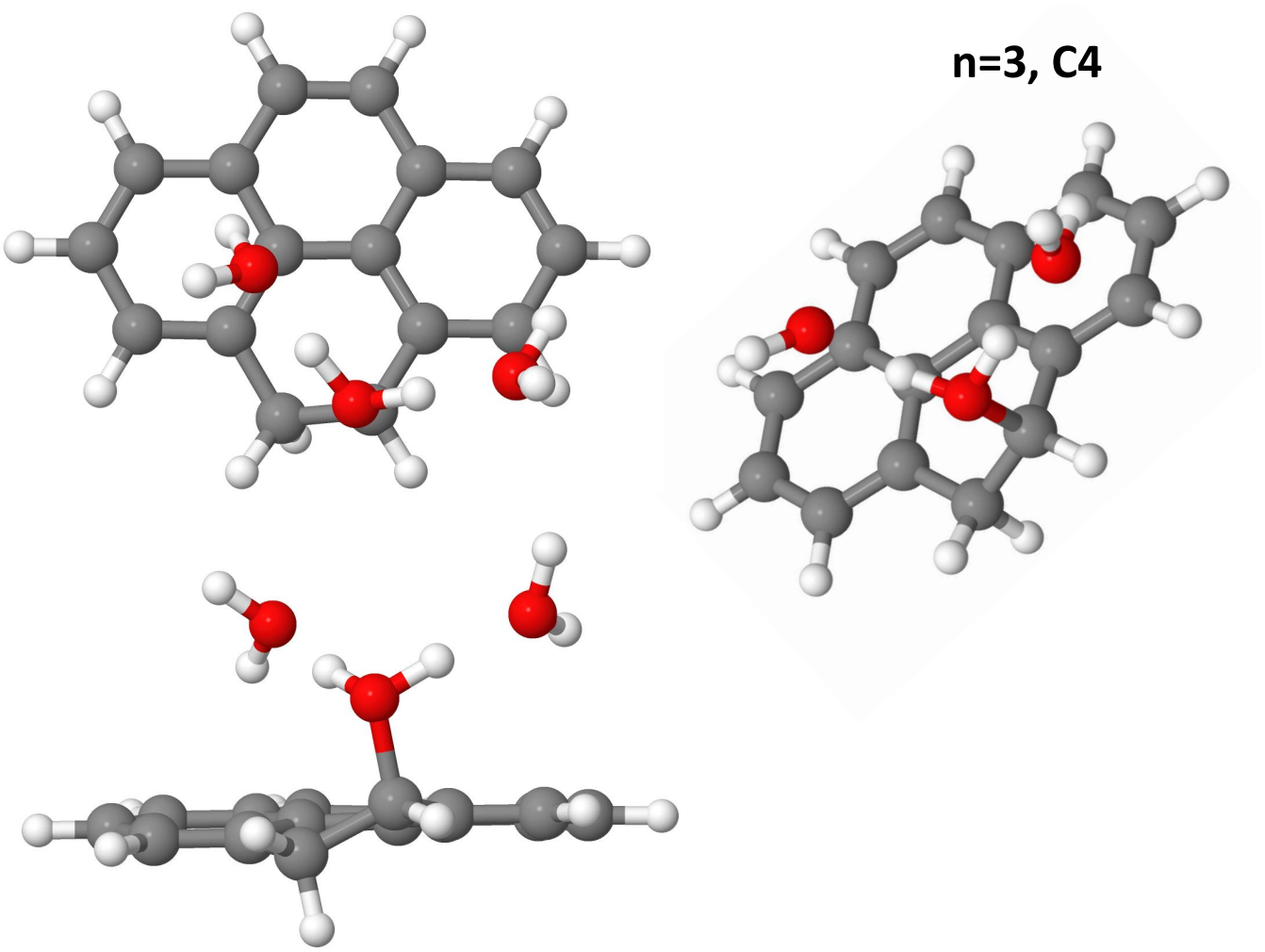

Figure S20: Different views corresponding to the lowest energy isomer obtained with a protonation site initially on C4 for n=3.

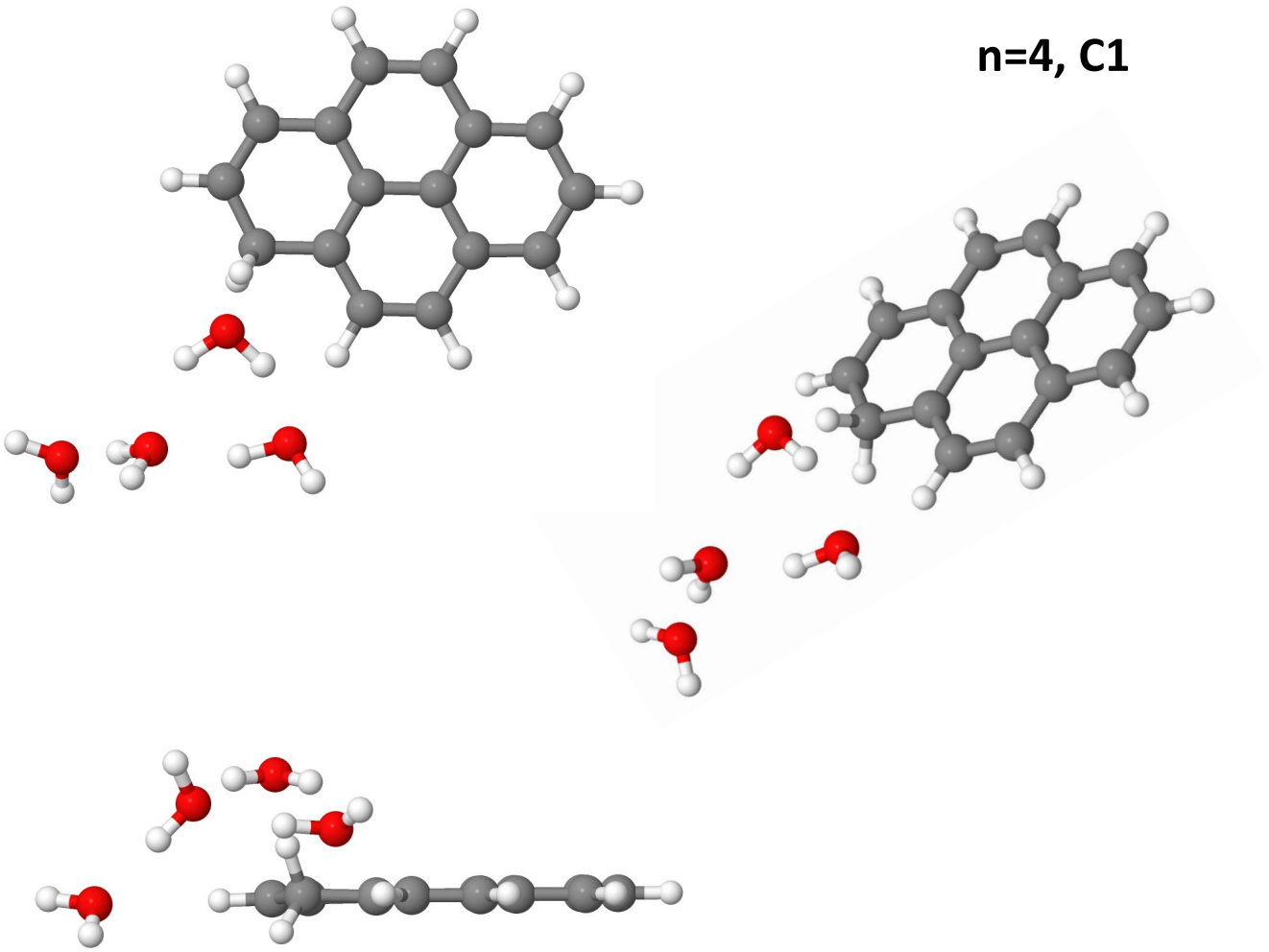

Figure S21: Different views corresponding to the lowest energy isomer obtained with a protonation site initially on C1 for n=4.

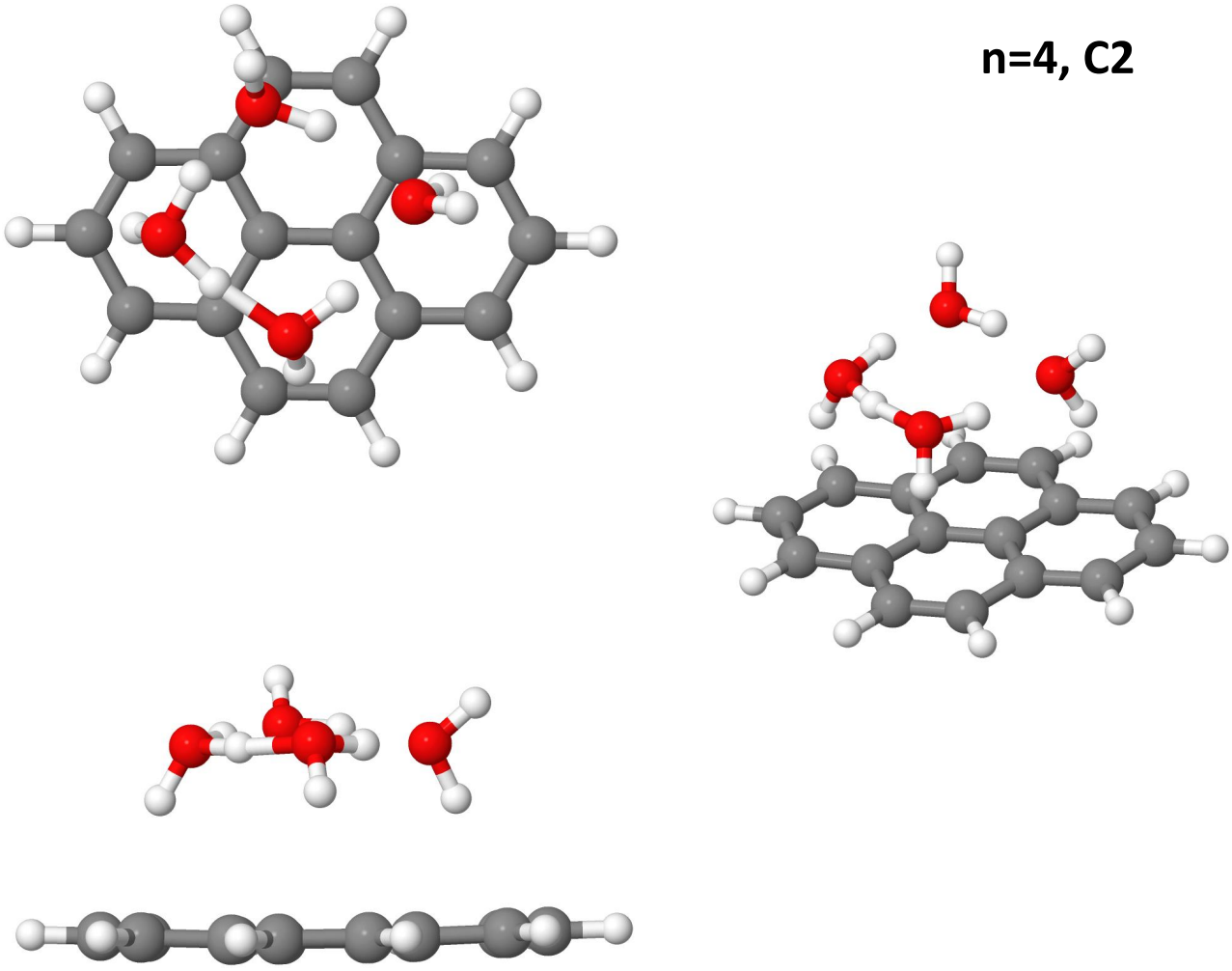

Figure S22: Different views corresponding to the lowest energy isomer obtained with a protonation site initially on C2 for n=4.

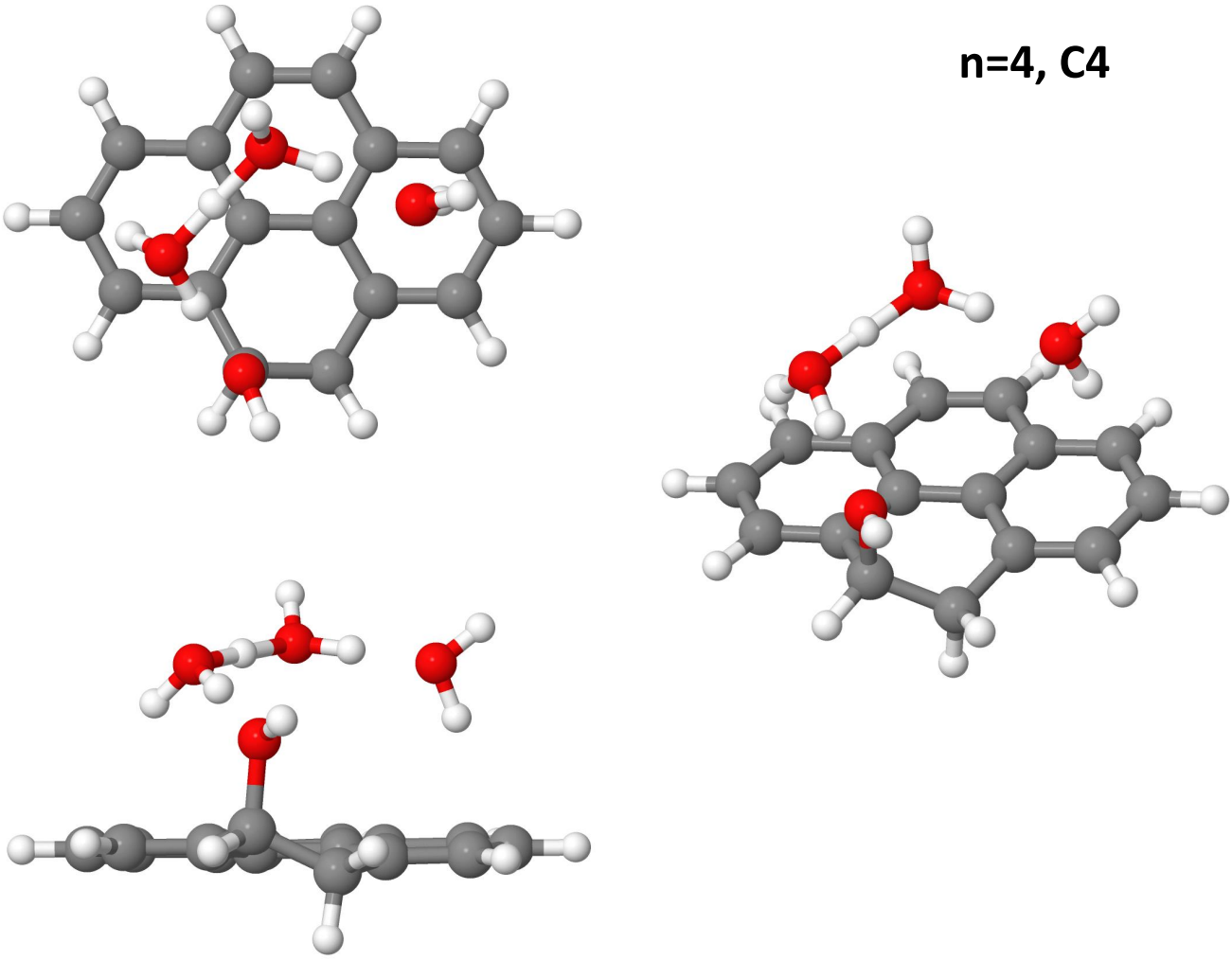

Figure S23: Different views corresponding to the lowest energy isomer obtained with a protonation site initially on C4 for n=4.

References

(1) Cheng, H.-P. Water Clusters: Fascinating Hydrogen-Bonding Networks, Solvation Shell Structures, and Proton Motion. *The Journal of Physical Chemistry A* **1998**, *102*, 6201–6204.

(2) Wròblewski, T.; Ziemczonek, L.; Karwasz, G. P. Proton transfer reactions for ionized water clusters. *Czechoslovak Journal of Physics* **2004**, *54*, C747.

(3) Kawai, Y.; Yamaguchi, S.; Okada, Y.; Takeuchi, K.; Yamauchi, Y.; Ozawa, S.; Nakai, H. Reactions of protonated water clusters H+(H2O)n (n=1–6) with dimethylsulfoxide in a guided ion beam apparatus. *Chemical Physics Letters* **2003**, *377*, 69–73.

(4) Goebbert, D. J.; Wenthold, P. G. Water Dimer Proton Affinity from the Kinetic Method: Dissociation Energy of the Water Dimer. *European Journal of Mass Spectrometry* **2004**, *10*, 837–845.

(5) Magnera, T. F.; David, D. E.; Michl, J. The first twenty-eight gas-phase proton hydration energies. *Chemical Physics Letters* **1991**, *182*, 363–370.

(6) Hunter, E. P. L.; Lias, S. G. Evaluated Gas Phase Basicities and Proton Affinities of Molecules: An Update. *Journal of Physical and Chemical Reference Data* **1998**, *27*, 413–656.

(7) Meot-Ner, M. Ion thermochemistry of low-volatility compounds in the gas phase. 3. Polycyclic aromatics: ionization energies, proton and hydrogen affinities. Extrapolations to graphite. *The Journal of Physical Chemistry* **1980**, *84*, 2716–2723.